06

Electronic structure of sintered zirconium carbide

© I.A. Shulepov, E.S. Mirovaya, A.A. Neiman, A.G. Burlachenko, S.P. Buyakova

Institute of Strength Physics and Materials Science, Siberian Branch, Russian Academy of Sciences,
634055 Tomsk, Russia
e-mail: shulepovia@ispms.ru

Received May 7, 2024
Revised July 4, 2024
Accepted July 7, 2024

The methods of electron spectroscopy, scanning electron microscopy and X-ray structural analysis were used to study samples of carbon, metallic zirconium and zirconium carbide. It was found that the studied samples exhibit differences in the Auger spectra and electron spectra of primary electrons of pure Zr and C and scattered on plasmons compared to ZrC. It was found that the average ionization potential of electrons in zirconium carbide was $\sim 7-10$ eV. Analysis of the results of X-ray diffraction, energy dispersive analysis and Auger spectrometry made it possible to determine the elemental and phase composition of zirconium carbide obtained by hot pressing. It was shown that the cubic lattice of ZrC contains impurity atoms of oxygen and nitrogen. It was found that the electrons of carbon in the composition of ZrC are at levels with a lower binding energy compared to their position in zirconium and carbon. It is suggested that the intensity of electrons scattered on plasmons decreases with increasing atomic density of the compound.

Keywords: Zirconium, carbon, zirconium carbide, Auger spectrometry, scattered electrons, spectrum, energy-dispersive analysis, scanning electron microscopy.

DOI: 10.61011/TP.2024.10.59359.118-24

Introduction

The physical and mechanical properties of zirconium carbide (ZrC) make it a promising material for use in products operating under high temperatures. It has both ceramic and metallic features, which include a high melting point (3540 °C), high hardness (up to 35 GPa), fine wear resistance, and high stability of characteristics at temperatures above 2000 °C. The techniques for production of solid ZrC and coatings from it and its physical and chemical properties have been studied for more than 50 years [1–6].

The authors of [1,4–6] used the methods of X-ray structural analysis, X-ray photoelectron and Auger spectroscopy, and scanning electron microscopy to develop new technological processes for ZrC production and predict its properties.

The chemical state of a ZrC coating deposited by the cathodic arc method was examined in [5] via X-ray photoelectron spectroscopy (XPS). The analysis of differences between XPS spectra of pure Zr and Zr in the carbide phase revealed the presence of a highly oxidized layer, which also contained carbon and oxygen as contaminants, on the surface of films. In addition, it was found that a certain fraction of carbon was not bound to Zr and did not form ZrC, and the bulk of the coating consisted of a mixture of ZrC (dominant phase), ZrO_2, and free carbon.

Samples of thin zirconium carbide films formed on Si (100) substrates by pulsed laser deposition in a CH_4 atmosphere were investigated in [7–9]. It was found that crystalline films could be grown only at laser fluences above 5 J/cm^2 and substrate temperatures higher than 500 °C. The electronic structure of the obtained films was not studied, and the methods of Auger electron spectroscopy (AES) and XPS were used only to determine the degree of surface contamination and the presence of oxygen in the films. It was found that the oxygen concentration decreased from 20 to $3-4$ atomic percent after sputtering a layer $3-5$ nm in thickness. Scanning electron microscopy (SEM) revealed that the films had a smooth surface with implied Rz roughness values below 1 nm. The mass density of the films was determined to be $6.32-6.57$ g/cm^3. A hardness of 27.6 GPa and a reduced elastic modulus of 228 GPa were determined as a result of nanoindentation tests for ZrC films deposited in an atmosphere of $2 \cdot 10^{-3}$ Pa CH_4.

The authors of [10] examined ZrCx samples, where x is molar ratio C/Zr = 0.84, 0.89, 0.95, 1.05, used in a gas-cooled high-temperature nuclear reactor. SEM and X-ray diffraction studies revealed that the samples with a high carbon concentration ($x = 0.95$, 1.05, and 1.17) contained a significant amount of graphite unbound with Zr atoms. The sample with $x = 0.89$ had the highest electron density corresponding to the highest carbon incorporation and the largest lattice parameter. An insignificant amount of oxygen was detected by AES.

The authors of [11] used AES to investigate powders of ZrC, ZrN, NbC, and NbN in cubic syngony. N(E) spectra were analyzed using the procedures of modeling and subtraction of the background of inelastically scattered electrons. Experimental KVV Auger spectra of non-metal atoms were compared with the results of calculations of the electronic structure of these compounds. It was determined how Auger spectra reflect the single-electron density of

states in the valence band; in addition, Auger spectra were compared to photoelectron spectra of the valence band that provide data on the electronic structure of the surface layer.

Having studied bulk ZrC samples, the authors of [12] concluded that the low-energy extremes near the 272 eV peak of the Auger spectrum of carbon are associated exclusively with the features of energy structure of the conduction band in zirconium carbide. It was found that the shape of Auger peaks of ZrC does not contradict the histogram of the density of electron states calculated by the tight binding method.

Auger spectra of reference samples of titanium, tungsten, and silicon carbides were analyzed in [13] to identify the structural features of Auger lines characteristic of these carbides. The integral $N(E)$ form of Auger spectra used in this study provides wider possibilities for determining the chemical state of elements and subsequent identification of phases than the differential $dN(E)/dE$ form.

High-resolution Auger spectra of niobium carbonitride NbC_xN_{1-x} (with $0.06 < x < 0.9$) were analyzed in [14] to study the electronic structure of these compounds. It was demonstrated that the local density of occupied states of nitrogen and carbon depends only weakly on the carbonitride composition, while the key changes in electronic structure with changing x are observed near the atoms of niobium.

The results of experimental and theoretical studies into the nature of structural vacancies in substoichiometric zirconium carbide (data on short-range and long-range ordering of vacancies, the mechanisms governing these phenomena, limitations in the fabrication of such structures, and the presently available information on thermophysical properties) were summarized in [15]. The authors of this review stress that the presence of nitrogen and oxygen impurities may (depending on their amount) affect significantly the stability of zirconium carbide, since they exert an influence on the ordering of vacancies.

It follows from the above that the analysis of secondary electron spectra provides an opportunity to probe changes in the electronic structure, which depends on the technological regimes of fabrication of articles and coatings from zirconium carbide. Therefore, one gets a chance to predict the properties of fabricated articles.

Thus, the aim of the present study is to examine the electronic structure of zirconium carbide with the use of secondary electron spectra of zirconium and zirconium carbide samples.

1. Materials and experimental procedure

Samples of metallic zirconium (Russia), graphite (Russia), and zirconium carbide were examined. Ceramic ZrC samples were prepared by hot pressing of powder (Russia; average particle size, $0.5 \pm 0.02\,\mu$m) at a temperature of 1900 °C and a pressure of 35 MPa in a protective atmosphere.

The chemical composition of surface layers of Zr, ZrC, and C was studied using a modernized 09-IOS-10 Auger spectrometer (Russia) [16]. The elemental composition of samples is determined in Auger spectrometry via ionization of the electron shells of atoms by primary electrons, subsequent recording of secondary electron spectra in the $N(E)$ and $dN(E)/dE$ forms, and isolation of energy lines characteristic of the atoms of elements that make up the sample under study. Secondary electron spectra were measured for parallelepiped-shaped samples $5 \times 8 \times 1$ mm in size, which were processed using the standard method for preparation of microsections.

These samples were positioned in the analytical chamber at the same level and were analyzed sequentially under the same spectrometer settings. The spectrometer parameters were as follows: primary electron energy, 3 keV; electron beam diameter, $20\,\mu$m; analyzed surface area, $200 \times 200\,\mu$m. Prior to measurements, the sample surface was sputtered to an atomically clean level with Ar^+ ions with an energy of 3 keV (to a depth of ~ 100 nm) incident at an angle of 70° relative to the normal to the surface. The sputtering process was continued during spectral measurements, but the current density was reduced to a value that excluded the adsorption of atoms from the residual atmosphere. A series of 10 spectra were recorded and averaged to exclude random errors. The background for experimental $N(E)$ spectra was modeled and subtracted using the Shirley method in AAnalyzer [17].

Microscopic images of the sample surfaces were obtained using Vega Tescan (Czech Republic) and LEO EVO 50 (Germany) scanning electron microscopes. The distribution of chemical elements was analyzed with a nitrogen-free Inca x-ACT (England) analytical drift detector.

Lattice parameters were determined using a Shimadzu diffractometer (Japan) with CuKα radiation. The „Match!" program (Germany) and Crystallography Open Database (COD) were used in X-ray analysis. The sizes of coherent scattering regions were calculated in accordance with the Scherrer formula based on the most intense diffraction peak. The lattice cell microdistortion was determined from broadening of the diffraction maximum at far diffraction angles.

2. Results

Figure 1 shows the survey secondary electron spectra of carbon, zirconium, and zirconium carbide in the dN/dE and $N(E)$ forms recorded within the energy interval from 0 to 500 eV. The spectra of Zr and ZrC were normalized to the highest intensity of the zirconium peak at 147 eV, and the intensity of the graphite peak at 270 eV was set equal to the intensity of the carbon peak in ZrC. It follows from the spectra in Fig. 1 that nitrogen and oxygen are present in Zr and ZrC; it should also be noted that the peaks in zirconium carbide located within the 31.5–120 eV interval are most intense than the peaks in zirconium. The higher resolution

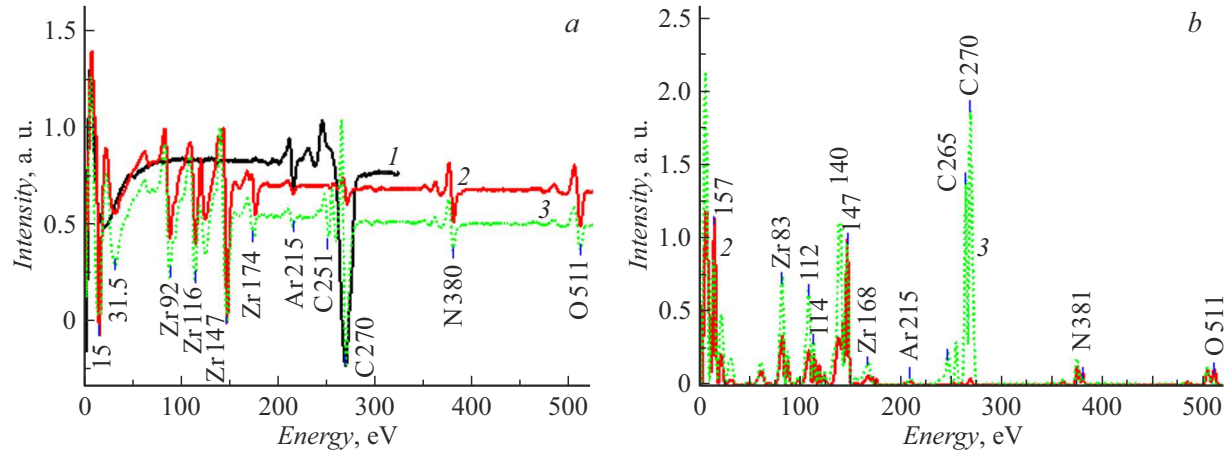

Figure 1. Survey secondary electron spectra: *a* — dN/dE; *b* — $N(E)$. *1* — Carbon, *2* — zirconium, and *3* — zirconium carbide.

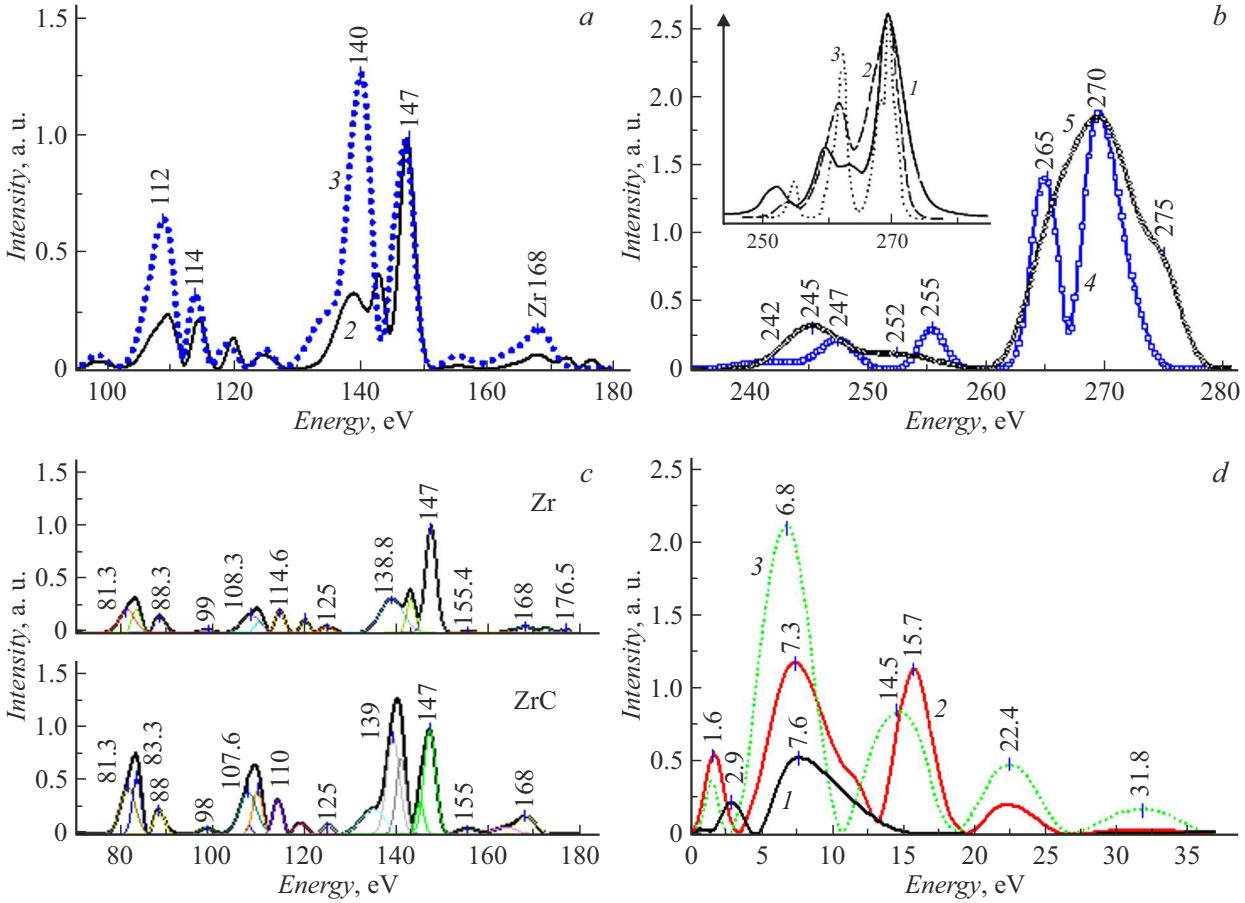

Figure 2. Sections of $N(E)$ secondary electron spectra: *a* — Zr (*2*) and ZrC (*3*); *b* — carbon *KVV* Auger spectra of ZrC (*4*) and graphite (*5*). The inset shows the data from [11]: experimental Auger spectrum of ZrC (*1*), self-convolution of the photoelectron spectrum of the valence band and the experimental Auger spectrum (*2*), and self-convolution of the experimental Auger spectrum and the total density of occupied states matched at the *pp* peak (*3*). *c* — Auger spectra and Gaussian components of Zr and ZrC; *d* — section of the spectra of C (*1*), Zr (*2*), and ZrC (*3*) extending from 0 to 37 eV.

of the $N(E)$ spectra (Fig. 1, *b*) allows one to identify lines that are not visible in Fig. 1, *a*.

Figure 2, *a* shows the 90–180 eV section of the $N(E)$ Auger spectra of pure zirconium (curve *2*) and zirconium in carbide (curve *3*). It can be seen that the Auger spectrum of Zr in ZrC differs in shape from the Auger spectrum of pure Zr and is significantly more intense. To obtain a quantitative estimate, the Auger spectra were integrated,

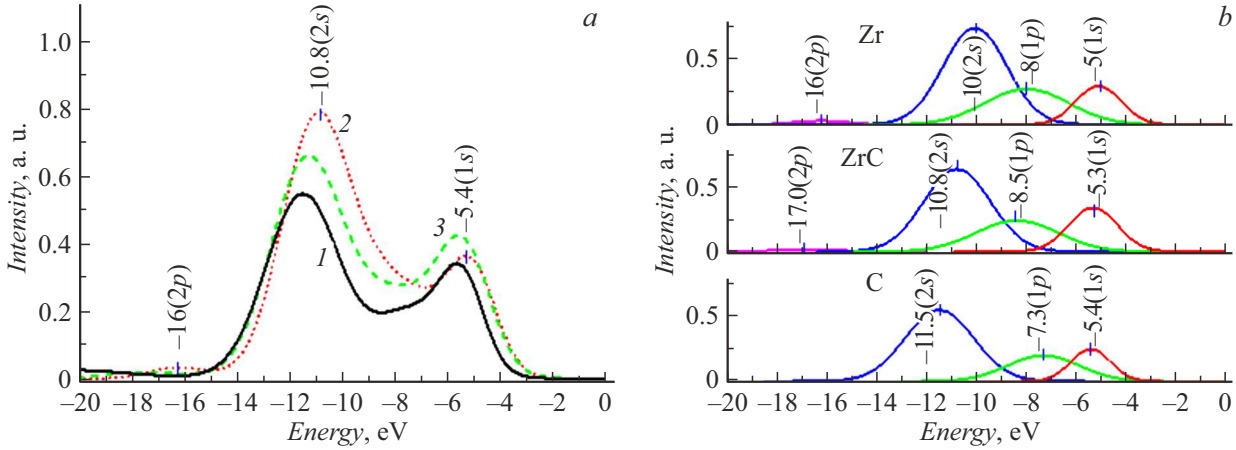

Figure 3. *a* — Spectra of discretely scattered electrons for *1* — C, *2* — Zr, and *3* — ZrC; *b* — Gaussian components of the spectra of discretely scattered electrons for C, Zr, and ZrC.

and the area difference was then calculated to be ~ 6.8. The Auger spectra (Fig. 2, *b*) of graphite (curve *5*) and carbon in zirconium carbide (curve *4*) also differ significantly; these spectra were integrated, and the area difference was found to be ~ 6.9. The deficiency in the spectrum of carbon in ZrC was ~ 6.9, and the excess in the spectrum of zirconium in ZrC was ~ 6.8.

A comparison with the Auger spectra of carbon presented in [11], which were measured for zirconium carbide powder and are shown in the inset of Fig. 2, *b*, revealed a close agreement with the results obtained in the present study in regard to the shape of the experimental spectrum (curve *1* in the inset) and the calculated spectrum (curve *3* in the inset).

In order to examine the structure of the Auger spectra of pure zirconium and zirconium carbide in more detail, the spectra were decomposed into Gaussian components (see Fig. 2, *c*). It can be seen that carbon facilitates the formation of electronic configurations contributing to the growth of intensities of certain lines of the Auger spectrum of Zr. One may identify changes in the electronic structure of zirconium and carbon atoms by analyzing the variation of intensities and energies of Gaussian components; however, it should be taken into account that the electronic spectra were measured for atoms in an excited state.

The measurement of high-resolution $N(E)$ spectra provides an opportunity to examine changes in the energy states of valence band electrons. Figure 2, *d* shows the section of spectra for C (curve *1*), Zr (curve *2*), and ZrC (curve *3*).

The spectra of electron energy losses due to scattering on plasmons are often used to identify changes in the chemical state of near-surface layers [18]. In the present study, we used the spectra of electrons scattered by plasmons measured in the process of irradiation of the sample surface with electrons with an energy of 1000 eV (Fig. 3, *a*). The peaks of energy loss at surface and bulk plasmons are denoted as *s* and *p*, respectively. The areas under the curves were integrated and were found to be 3.64 for carbon (curve *1*), 4.39 for zirconium (curve *2*), and 4.16 for zirconium carbide (curve *3*). The results obtained for zirconium, zirconium carbide, and graphite after normalization to the maximum intensity and decomposition into Gaussian components are presented in Fig. 3, *b*. The areas under the 1*s*, 1*p*, and 2*s* curves and the values of ratio $2s/1s$ are listed in Table 1.

Table 1. Intensities of electrons scattered on *s* and *p* plasmons for Zr, C, and ZrC

Plasmons	Intensities of discretely scattered electrons, a. u.		
	Zr	C	ZrC
1*s*	0.68	0.5	0.84
1*p*	1.17	0.73	1.01
2*s*	2.36	1.9	2.13
Ratio $2s/1s$	3.5	3.8	2.5

Secondary ion-electron emission (SIEE) spectra supplement data on the electronic structure of near-surface layers of solids [19]. These spectra were recorded in the process of sputtering of Zr, ZrC, and C surfaces with argon ions with an energy of 3000 eV (Fig. 4, *a*). The areas under the experimental curves were 5.54 for zirconium (curve *1*), 2.47 for zirconium carbide (curve *2*), and 0.85 for carbon (curve *3*). To evaluate the differences between the spectra, the obtained curves were normalized to the highest intensities and decomposed into Gaussian components (Fig. 4, *b*), which were integrated. The integration results are presented in Table 2.

The X-ray diffraction patterns of bulk samples of C, Zr, and ZrC are shown in Fig. 5. It was found that zirconium had a hexagonal structure with lattice param-

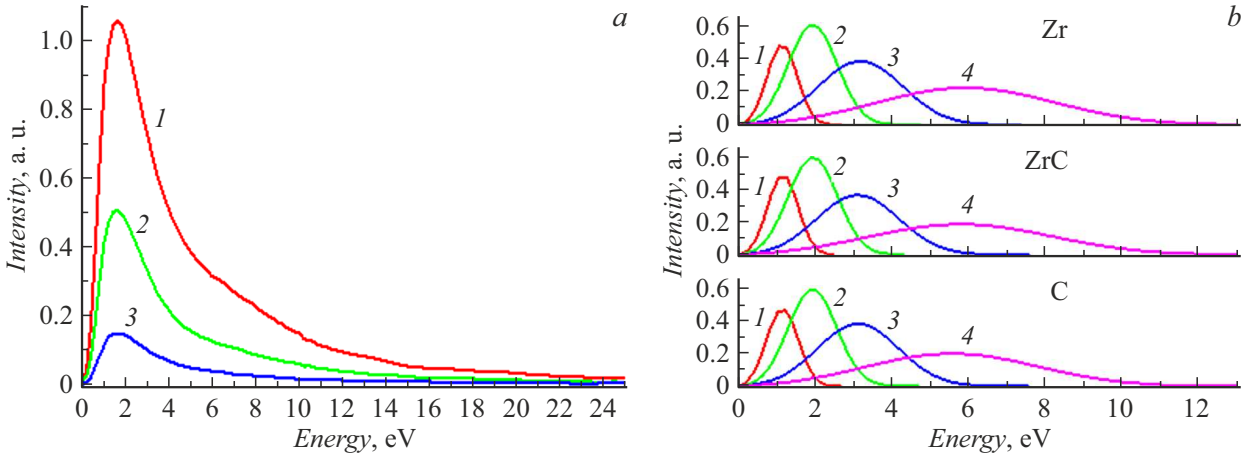

Figure 4. *a* — Energy spectra of electrons recorded under excitation of the surfaces of Zr (*1*), ZrC (*2*), and C (*3*) by Ar^+ (3000 eV) ions; *b* — spectra decomposed into Gaussians with preliminary normalization to the highest intensity.

Table 2. Intensities of the Gaussian components in Fig. 4, *b*

Samples			
Lines	Gaussian intensity, a. u.		
	Zr	ZrC	C
1	0.47	0.48	0.48
2	0.96	0.95	0.93
3	1.05	0.97	1.0
4	1.28	1.08	1.09

eters $a = 0.3222$ nm and $c = 0.51334$ nm. Carbon had a hexagonal structure (it was impossible to determine the lattice parameters of graphite, since only two peaks were recorded in the X-ray diffraction pattern). The X-ray diffraction pattern of the zirconium carbide sample featured the basic set of reflections of cubic ZrC and low-intensity peaks of the monoclinic phase of zirconium dioxide. Zirconium carbide was characterized by a face-centered cubic lattice with a parameter of 0.4665 nm. It is worth noting that the calculated lattice parameter of ZrC differs from literature data, which may be attributed both to the stoichiometry of ZrC and to the presence of impurities in the lattice cell. Specifically, the range of a values for zirconium carbide ZrC_{1-x} is 0.4652–0.478 nm [20]. This wide variation of lattice parameter values may be dictated by dissolved oxygen and/or nitrogen with subsequent substitution of carbon atoms in the zirconium carbide structure, which leads to the formation of oxycarbides $ZrC_{1-x}O_y$, carbonitrides $ZrC_{1-x}N_z$, and, most often, oxycarbonitride $ZrC_{1-x}N_zO_y$ phases. It should be noted that the presence of nitrogen and/or oxygen impurities may (depending on their amount) affect significantly the stability of zirconium carbide, since they exert an influence on the ordering of vacancies [20]. A comparison with literature data revealed that the calculated lattice parameter of 0.4665 nm corresponds to $ZrC_{0.65}O_{0.03}$ [21].

SEM images of the surfaces of C, Zr, and ZrC samples are shown in Fig. 6. Uniform porosity is seen on the surface of zirconium carbide and zirconium, and polyhedral grains are visible on the surface of graphite.

Table 3 presents the concentrations of elements (in atomic percent) determined by EDS and Auger spectroscopy with the use of standard elemental sensitivity coefficients [22]. Nitrogen was not detected by EDS due to the overlap of the energy lines of nitrogen and oxygen. The differences in concentration may be attributed to the specifics of preliminary preparation of the analyzed surface. Specifically, the standard method for preparation of microsections was used in EDS analysis without additional surface cleaning procedures, while the surface of samples subjected to Auger analysis was sputtered in the analytical chamber with Ar^+ ions to an atomically clean level.

3. Discussion

According to the results of XPS and Auger studies of zirconium carbide reported in [5,9], the spectra of zirconium in pure form and as a part of ceramics did not have any significant differences. Therefore, the changes in electronic states were assessed by examining the spectra of carbon. In the present study, the shapes of experimental spectra of carbon and zirconium in pure form and as part of carbide were found to be different. The validity of spectral measurements is verified by the presence of three groups of peaks in the Auger spectrum of zirconium (176, 114, 88 eV), which corresponds to the contribution of core levels $3d$ (179−181 eV), $3p$ (330−343 eV), and $3s$ (430 eV) [23]. The energies of the final states of the Auger transition were calculated in accordance with formula (1) [24] (the electron

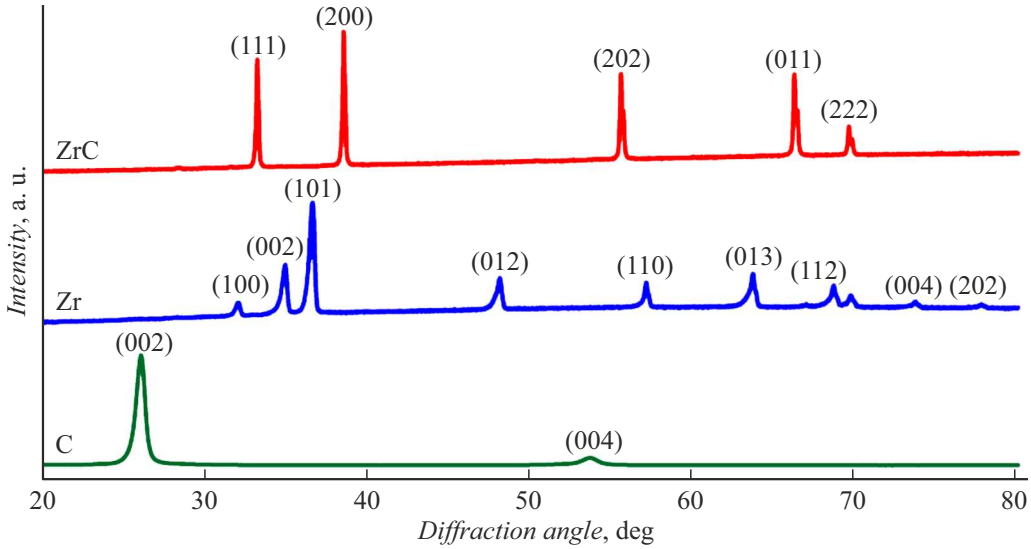

Figure 5. X-ray patterns of graphite, zirconium, and zirconium carbide.

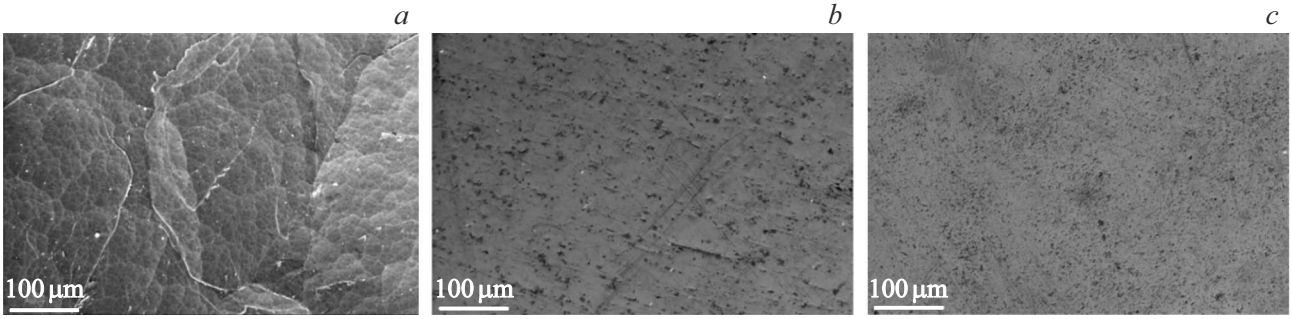

Figure 6. SEM images of surfaces: *a* — graphite, *b* — zirconium, and *c* — zirconium carbide.

Table 3. Atomic percentage of elements determined by Auger spectroscopy and energy-dispersive X-ray spectroscopy

Sample	Zr				ZrC			
Measurement units, %	Atomic		Weight		Atomic		Weight	
Method	Auger	EDS	Auger	EDS	Auger	EDS	Auger	EDS
Zr	78.7	72.1	96.0	93.7	49.2	41.6	87.7	82.6
C	7.1		1.1		43.3	45.3	10.2	13.6
N	7.9		1.5		4.3		1.1	
O	6.3	27.9	1.4	6.3	3.2	13.2	1.0	3.8

binding energies are given in Table 4). The obtained results are presented in Table 5.

$$E^Z_{\alpha\beta\gamma} = E^Z_\alpha - E^Z_\beta - E^Z_\gamma - \frac{1}{2}\left(E^{Z+1}_\gamma - E^Z_\gamma + E^{Z+1}_\beta - E^Z_\beta\right), \quad (1)$$

where $E^Z_{\alpha\beta\gamma}$ is the energy of Auger transition $\alpha\beta\gamma$ in element Z. The first three terms correspond to the binding energy of shells; since correction term $\frac{1}{2}\left(E^{Z+1}_\gamma - E^Z_\gamma + E^{Z+1}_\beta - E^Z_\beta\right)$ is small, it is neglected in the present case.

It follows from the calculated data (Table 5) that the peaks at 255, 265, and 270 eV (Fig. 2, *b*) are induced by Auger transitions KL_1L_1, KL_1L_2, and KL_2L_2, respectively. Other peaks form due to excitation and ionization of electron shells of atoms by electrons and hybridization of orbitals with the emergence of various configurations. This leads to the formation of peaks with energies of

Table 4. Electron binding energies [24]

	X-ray level designation (AES)												
	K	L_1	L_2	M_1	M_2	M_3	M_4	M_5	N_1	N_2	N_3	N_4	N_5
	Spectroscopic level designation (XPS)												
	$1s_{1/2}$	$2s_{1/2}$	$2p_{1/2}$	$3s_{1/2}$	$3p_{1/2}$	$3p_{3/2}$	$3d_{3/2}$	$3d_{5/2}$	$4s_{1/2}$	$4p_{1/2}$	$4p_{3/2}$	$4d_{3/2}$	$4d_{5/2}$
Element	Binding energies, eV												
C	284	14	7										
Zr				431	345	331	183	180	52	29	27.1	3	3
N	399	19	9										
O	535	24	7										

Table 5. Energies and Auger transitions for carbon and zirconium

Element	Auger transition	Energy $E^Z_{\alpha\beta\gamma}$, eV	Calculated $E^Z_{\alpha\beta\gamma}$, eV
C	KM_1M_1	242	$284(K) - 21(2s^2) - 21(2s^2) = 242$
	$KM_{2,3}M_{2,3}$	245	$284(K) - 19(2p^3) - 19(2p^3) = 246$
	$KM_{2,3}M_{2,3}$	247	$284(K) - 18(2p^3) - 18(2p^3) = 248$
	KL_1L_1	255	$284(K) - 14(L_1) - 14(L_1) = 256$
	KL_1L_2	265	$284(K) - 14(L_1) - 7(L_2) = 263$
	KL_2L_2	270	$284(K) - 7(L_2) - 7(L_2) = 270$
	$KL_2L_1(2s^22p^2)$	275	$284(K) - 7(L_2) - 2(2s^22p^2) = 275$
Zr	$M_1M_4M_4$	62	$430(M_1) - 181(M_4) - 181(M_4) = 68$
	$M_1M_2M_4$	83	$430(M_1) - 343(M_2) - 3(N_{40,86,5}) = 84$
	$M_5N_1\left(\frac{4p^34d}{4p^55s}\right)$	88	$179(M_5) - 51(N_1) - 40(4p^34d) = 88(4p^55s)$
	$M_2M_4N_1$	110	$343(M_2) - 181(M_4) - 51(N_1) = 111$
	$M_2M_5N_1$	114	$343(M_2) - 179(M_5) - 51(N_1) = 113$
	$M_3M_4N_{2,3}$	120	$330(M_3) - 181(M_4) - 28(N_{2,3}) = 121$
	$M_5N_{1,2}N_{2,5}$	125	$179(M_5) - 28(N_2) - 28(N_2) = 123$ $179(M_5) - 51(N_1) - 3(N_5) = 125$
	$M_2M_5N_2$	139	$343(M_2) - 179(M_5) - 28(N_2) = 136$
	$M_3M_4N_5$	143	$330(M_3) - 181(M_4) - 3(N_5) = 146$
	$M_{3,5}N_5N_4$	147	$179(M_5) - 28(N_{2,3}) - 3(N_{4,5}) = 148$ $330(M_3) - 179(M_5) - 3(N_{4,5}) = 148$
	$M_{4,5}N_5N_4$	176	$179(M_5) - 3(N_5) - 3(N_5) = 173$ $181(M_4) - 3(N_5) - 3(N_5) = 175$

245 eV ($2p^3 - 19$ eV) and 275 eV $2s^22p^2$ (1–3 eV) [25] for carbon in graphite and 242 eV ($2s^2 - 21$ eV) and 247 eV ($2p^3 - 18$ eV) (Table 5) for carbon in zirconium carbide. In the Auger spectrum of graphite, the peaks at 255, 265, and 270 eV merge, forming a broad spectrum (curve *5* in Fig. 2, *b*). Separate peaks form at 255, 265, and 270 eV in ZrC, which is reflected in the spectrum (Fig. 2, *b*, curve *4*). The 275 eV peak is lacking in zirconium carbide, since the *d* subband is not filled [14]. The electronic spectra in Figs. 1, 2 demonstrate that the electrons of carbon atoms in zirconium carbide alter significantly the shape of electronic spectra of zirconium. This is likely to be

caused by the transition of carbon electrons in zirconium carbide to levels with a lower binding energy, which enables interatomic Auger transitions [26–29]. This is verified by the difference in areas under the Auger lines of zirconium and carbon determined above. The difference is approximately the same for Zr and C and amounts to ~ 6.8 (excess) and ~ 6.9 (deficiency). The spectra in Fig. 2, *d* make it clear how the structure of the valence band of ZrC is formed from the electrons of zirconium and carbon atoms. The electron binding energy decreased (the spectrum is shifted toward lower energies (curve *3*)), while the intensity (related to the number of electrons) increased, contributing to the emergence of interatomic Auger transitions.

The energy loss spectra shown in Fig. 3, *a* indicate that the number of plasmons (related to the intensity of the spectra) formed on the surface depends on the electron gas density (which, in turn, depends on the atomic density), and the lower the atomic density ($4.29 \cdot 10^{22}$ at/cm^2 for Zr and $1.76 \cdot 10^{23}$ at/cm^2 for C) is, the higher is the intensity of discretely scattered electrons. The atomic density of ZrC is higher than the one of Zr, which is confirmed by X-ray diffraction data. The shift of peaks toward lower energies is also associated with atomic density, which contributes to a reduction in energy (oscillation frequency of plasmons). The $2s/1s$ intensity ratio (Fig. 3, *b*, Table 1) is 3.5 for Zr and 2.5 for ZrC. Therefore, the concentration of electrons in surface plasmons of ZrC is greater than in Zr, and this, as was said above, is associated with the higher atomic density of ZrC.

The mechanism of secondary ion-electron emission was discussed in [30]. It was demonstrated that SIEE is characterized by coefficient γ, which is the average number of electrons escaping into vacuum per incident particle with a given energy E_0, and distribution $N_0(E_k)$ of these electrons in kinetic energy E_k outside the solid. Both these parameters depend on the properties of the bombarded object and the incident particles (including their kinetic energy). The spectra of electrons emitted by Ar^+ ions in the process of sputtering of the sample surfaces (see Fig. 4, *a*) demonstrate that average number N_0 of electrons escaping into vacuum is the highest for Zr (with an atomic density of $4.29 \cdot 10^{22}$ at/cm^2) and the lowest for C (with an atomic density of $1.76 \cdot 10^{23}$ at/cm^2). Thus, it is fair to assume that the SIEE intensity in this case is the highest for the sample with a lower atomic density. SIEE is induced by the potential and kinetic (impact) breaking-away of electrons by bombarding ions. Electrons of surface atoms with energies up to 5 eV are released into vacuum as a result of potential breaking-away. Since the SIEE intensity (Fig. 4, *a*) is associated, among other things, with the ionization potentials of atoms, it may be concluded that the ionization potential of ZrC is $\sim 7 - 10$ eV, since the ionization potential for C and Zr is 11.2 and 6.63 eV, respectively [31]. To identify the contribution of electrons from different energy levels to SIEE, we examine the spectra in Fig. 4, *b* and the data in Table 2. The intensities of lines *1*–*3* with energies of 1, 2, and 2.5 eV, respectively, are virtually indistinguishable, since they are formed due largely to potential ionization, and the intensity of line *4* (6 eV) receives an additional contribution from kinetic ionization (the efficiency of which is higher for Zr, since it has a lower atomic density).

Conclusion

It follows from the analysis of electronic spectra that the energy states of valence-band electrons of carbon and zirconium atoms in zirconium carbide are altered via transitions to levels with a lower binding energy, which contribute to the emergence of interatomic Auger transitions.

It was demonstrated that the ratio of formation probabilities of 2*s* and 1*s* plasmons on the surface of zirconium is higher than on the surface of zirconium carbide. Since the atomic density of ZrC is higher than the one of Zr, it is natural to assume that the lower the atomic density is, the higher is the intensity of discretely scattered electrons.

The examination of variations of ion-electron spectra revealed that the average ionization potential of electrons in zirconium carbide is $\sim 7 - 10$ eV, whereas the same potential in Zr is 6.63 eV.

The results of joint Auger and EDS studies revealed the presence of oxygen (6.3 and 3.2 at.%) and nitrogen (7.9 and 4.3 at.%) in Zr and ZrC, respectively.

Acknowledgments

The authors wish to thank V.V. Knutarev for his assistance in this work.

Funding

This study was carried out under the state assignment of the Institute of Strength Physics and Materials Science of the Siberian Branch of the Russian Academy of Sciences, project No. FWRW-2021-0009.

Conflict of interest

The authors declare that they have no conflict of interest

References

[1] T.I. Alekseeva, G.V. Galevskii, V.V. Rudneva, S.G. Galevskii. Nauchno-Tekh. Vedomosti S.-Peterb. Gos. Politekh. Univ., **23** (1), 2017, 256 (2017) (in Russian). DOI: 10.18721/JEST.230126

[2] T.I. Alekseeva, G.V. Galevskii, V.V. Rudneva. Vestn. Gorno-Metall. Sekts. Ross. Akad. Estestv. Nauk. Otd. Metall., 36, 136 (2016) (in Russian).

[3] T.I. Alekseeva, G.V. Galevskii, V.V. Rudneva, S.G. Galevskii. Vestn. Irkutsk. Gos. Tekh. Univ., **22** (7), 164 (2018) (in Russian). DOI: 10.21285/1814-3520-2018-7-164-180

[4] D.C. Smith, R.R. Rubiano, M.D. Healy, R.W. Springer. *Low-Temperaturedeposition of ZrC thin Films from a Single Source Precursor*. Los Alamos National Laboratory, Los Alamos, NM 87545 Department of Nuclear Engineering, MIT, Cambridge, MA 02139. Mat. Res. Soc. Symp. Proc. V. 282. 1993 Materials Research Society. P. 643–649.
[5] M. Balaceanu, M. Braic, V. Braic, A. Vladescu, C.C. Negrila. J. Optoelectronics and Advanced Mater., **7** (5), 2557 (2005).
[6] D. Craciun, G. Socol, E. Lambers, E.J. McCumiskey, C.R. Taylor, C. Martin, N. Argibay, D.B. Tanner, V. Craciun. Appl. Surface Sci., **352**, *28* (2015).
[7] V. Craciun, D. Craciun, J.M. Howard, J. Woo. Thin Solid Films, **515**, 4636 (2007). DOI: 10.1016/j.tsf.2006.11.122
[8] D. Craciun, G. Socol, N. Stefan, I.N. Mihailescu, G. Bourne, V. Craciun. Surf. Coatings Technol., **203**, 1055 (2009). DOI: 10.1016/j.surfcoat.2008.09.039
[9] D. Craciun, G. Socol, N. Stefan, G. Bourne, V. Craciun. Appl. Surf. Sci., **255**, 5260 (2009). DOI: 10.1016/j.apsusc.2008.08.097
[10] G.W.Ch. Silva, A.A. Kercher, J.D. Hunn, R.C. Martin, G.E. Jellison, H.M. Meyer. J. Solid State Chem., **194**, 91 (2012). DOI: 10.1016/j.jssc.2012.04.047
[11] Yu.M. Shul'ga, V.I. Rubtsov, Yu.G. Borod'ko. Poverkhnost', **8**, 43 (1987) (in Russian).
[12] T.L. Matskevich, A.P. Kazantsev. Fiz. Tverd. Tela, **20** (11), 3365 (1978) (in Russian).
[13] T.N. Smetyukhova, A.V. Druzhinin, D.A. Podgorny. J. Surf. Invest.: X-Ray, Synchrotron Neutron Tech., **11**, 414 (2017). DOI: 10.7868/S0207352817040163
[14] V.I. Rubtsov, Yu.M. Shul'ga. Fiz. Tverd. Tela, **32** (5), 1323 (1990) (in Russian).
[15] T. Davey, Y. Chen. Int. J. Ceramic Eng. Sci., **4**, 134 (2022). DOI: 10.1002/ces2.1012
[16] V.E. Panin, I.A. Shulepov, N.A. Narkevich, L.B. Botaeva. Phys. Mesomech., **24** (2), 131 (2021).
[17] AAnalyzer: a peak-fitting program for photoemission data. Electronic source. Available at: https://xpsoasis.org/aanalyzer_manual
[18] A.S. Parshin, G.A. Aleksandrova, A.V. Zyuganova. J. Surf. Invest.: X-Ray, Synchrotron Neutron Tech., **1**, 323 (2007).
[19] N. Benazeth. Nucl. Instrum. Methods in Phys. Res., **194** (1–3), 405 (1982).
[20] I.L. Shabalin. *Ultra-High Temperature Materials II: Refractory Carbides I (Ta, Hf, Nb and Zr Carbides)* (Springer, 2019), DOI: 10.1007/978-94-024-1302-1
[21] G.V. Samsonov, M.S. Koval'chenko, R.Ya. Petrykina, V.Ya. Naumenko. Soviet Powder Metallurgy and Metal Ceramics, **9** (9), 713 (1970). https://link.springer.com/article/10.1007/bf00836960#preview
[22] L.E. Davis, N.C. MacDonald, P.W. Palmberg, G.E. Riach, R.E. Weber. *Handbook of Auger Electron Spectroscopy. A Reference Book of Standard Data for Identification and Interpretation of Auger Electron Spectroscopy Data. Second edition.* (Physical Electronics Division Perkin·Elmer Corporation, USA), https://www.cnyn.unam.mx/ wencel/XPS/MANAES2.pdf
[23] J.F. Moulder, W.F. Stickle, P.E. Sobol, K.D. Bomben. *Handbook of X-ray Photoelectron Spectroscopy A Reference Book of Standard Spectra for Identification and Interpretation of XPS Data.* Edited by Jill Chastain (Perkin-Elmer Corporation Physical Electronics Division, USA), https://www.cnyn.unam.mx/ wencel/XPS/MANXPS.pdf
[24] L.C. Feldman, J.W. Mayer. *Fundamentals of Surface and thin Film Analysis* (North-Holland–NY.–Amsterdam–London, 1986)
[25] Information system „Electronic Structure of Atoms." http://grotrian.nsu.ru/ru
[26] P.H. Citrin. Phys. Rev. Lett., **31** (19), 1164 (1973). https://journals.aps.org/prl/pdf/10.1103/PhysRevLett.31.1164
[27] J.A.D. Matthew, Y. Komninos. Surf. Sci., **53** (1), 716 (1975). DOI: 10.1016/0039-6028(75)90166-1
[28] Lo I. Yin, T. Tsang, G.J. Coyle, W. Yin, I. Adler. J. Vac. Sci. Technol., **1** (2), 1000 (1983). DOI: 10.1116/1.572323
[29] V.I. Grebennikov, T.V. Kuznetsova. J. Surf. Invest.: X-Ray, Synchrotron Neutron Tech., **14**, 494 (2020). https://scientificrussia.ru/articles/rezultiruyushchij-spektr-magnitnyh-momentov
[30] I.A. Abroyan, M.A. Eremeev, N.N. Petrov. Sov. Phys. Usp., **10** (3), 332 (1967). https://ufn.ru/ufn67/ufn67_5/Russian/r675e.pdf
[31] A.I. Volkov, I.M. Zharskii. *Bol'shoi khimicheskii spravochnik* (Sovrem. Shkola, Minsk, 2005) (in Russian).

Translated by D.Safin